







RESEARCH ARTICLE

Rapid ex vivo reverse genetics identifies the essential determinants of prion protein toxicity

Regina R. Reimann¹  | Martina Puzio¹  | Antonella Rosati¹ |
 Marc Emmenegger¹  | Bernard L. Schneider²  | Pamela Valdés² |
 Danzhi Huang³ | Amedeo Caflich³  | Adriano Aguzzi¹ 

¹Institute of Neuropathology, University of Zurich, Zurich, Switzerland

²Brain Mind Institute, Ecole Polytechnique Fédérale de Lausanne, Lausanne, Switzerland

³Department of Biochemistry, University of Zürich, Zürich, Switzerland

Correspondence

Adriano Aguzzi and Regina R. Reimann, Institute of Neuropathology, University of Zurich, Schmelzbergstrasse 12, CH-8091 Zurich, Switzerland.
 Email: adriano.aguzzi@usz.ch and regina.reimann@usz.ch

Funding information

Georg und Bertha Schwyzer-Winiker-Stiftung; H2020 European Research Council (ERC Prion2020), Grant/Award Number: 670958; Human Frontier Science Program, Grant/Award Number: ID RGP0001/2022; Innosuisse - Schweizerische Agentur für Innovationsförderung, Grant/Award Number: 100.020 IP-LS; Innovation Fund of the University Hospital Zurich, Grant/Award Number: INOV00096; Michael J. Fox Foundation for Parkinson's Research, Grant/Award Number: ID MJFF-022156; René Baumgart-Stiftung, Grant/Award Number: USZF27101; Schweizerischer Nationalfonds zur Förderung der Wissenschaftlichen Forschung, Grant/Award Numbers: ID 179040, ID 207872, ID 183563; Swiss Personalized Health Network, Grant/Award Number: 2017DRI17; Stavros Niarchos Foundation

Abstract

The cellular prion protein PrP^C mediates the neurotoxicity of prions and other protein aggregates through poorly understood mechanisms. Antibody-derived ligands against the globular domain of PrP^C (GDL) can also initiate neurotoxicity by inducing an intramolecular R₂₀₈-H₁₄₀ hydrogen bond (“H-latch”) between the α₂-α₃ and β₂-α₂ loops of PrP^C. Importantly, GDL that suppresses the H-latch prolong the life of prion-infected mice, suggesting that GDL toxicity and prion infections exploit convergent pathways. To define the structural underpinnings of these phenomena, we transduced 19 individual PrP^C variants to PrP^C-deficient cerebellar organotypic cultured slices using adenovirus-associated viral vectors (AAV). We report that GDL toxicity requires a single N-proximal cationic residue (K₂₇ or R₂₇) within PrP^C. Alanine substitution of K₂₇ also prevented the toxicity of PrP^C mutants that induce Shmerling syndrome, a neurodegenerative disease that is suppressed by co-expression of wild-type PrP^C. K₂₇ may represent an actionable target for compounds aimed at preventing prion-related neurodegeneration.

KEYWORDS

neurodegeneration, prion disease, reverse genetic

1 | INTRODUCTION

The structure of the cellular prion protein PrP^C encompasses an amino-proximal flexible tail (FT, amino acid residues 23–123) linked to a globular domain (GD, 124–230) [1]. PrP^C triggers a neurotoxic cascade upon interaction with prions [2–4], other pathological protein aggregates including Aβ [5–7], and antibodies or antibody-derived ligands against its globular domain

(henceforth collectively called globular-domain ligands or GDL) [8–11]. In addition, PrP^C mutants carrying deletions of certain domains induce severe neurodegeneration, which can be suppressed by co-expression of wild-type (wt) PrP^C [12–14].

Others and we have found that ligands targeting the α₁ and α₃ helices of the GD, or the second charge cluster (CC2: 95–110), induce an acute neurodegenerative phenotype [8, 10, 11] resembling that of prion infections [15].

This is an open access article under the terms of the [Creative Commons Attribution-NonCommercial-NoDerivs](https://creativecommons.org/licenses/by-nc-nd/4.0/) License, which permits use and distribution in any medium, provided the original work is properly cited, the use is non-commercial and no modifications or adaptations are made.

© 2022 The Authors. *Brain Pathology* published by John Wiley & Sons Ltd on behalf of International Society of Neuropathology.

TABLE 1 Summary prion protein constructs

Symbol	Description	Characteristics	Expression
PrPΔ23–31	Deletion from position 23 to 31	Deletion of polybasic region	Figures S6A and S8A
PrPΔ28–49	Deletion from position 28 to 49	Deletion preceding the octapeptide repeat region	Figures S6A and S8A
PrPΔ32–93	Deletion from position 32 to 93	Depletion of octapeptide repeat and its preceding region	Figures S6C and S8C
PrPΔ50–90	Deletion from position 50 to 90	Deletion of octapeptide repeat	Figures S6A and S8A
PrPΔ94–110	Deletion from position 94 to 110	Deletion of second charge cluster	Figures S6A and S8A
PrPΔ111–134	Deletion from position 111 to 134	Deletion of hydrophobic core	Figures S6A and S8A
PrP K → A 23–27	Triple lysine to alanine at position 23, 24, 27	Decrease of positive charge of CC1 by three lysines	Figures S6B and S8B
PrP K → A 23–24	Double lysine to alanine at position 23, 24	Decrease in positive charge of CC1 by two lysines at the start of the flexible tail	Figures S6B and S8B
PrP K → A 27	Lysine to alanine mutation at position 27	Decrease in positive charge at position 27 of CC1	Figures S6B and S8B
PrP K → R 23–27	Triple lysine to arginine at position 23, 24, 27	Intact charged CC1	Figures S6B and S8B
PrP inv50–90	Inversion of the sequence from AA 50 to 90	Intact physical properties but altered interaction capabilities with ionic or proteinaceous binding partners of the octapeptide region	Figures S6C and S8C
PrP Inv(52–55/60–63/68–71/76–79/84–87)	Five point inversions: 52–55; 60–63; 68–71; 76–79; 84–87	Inversion of amino acid stretch in between repetitive WGQP motif of octapeptide region	Figures S6C and S8C
PrP Trans(56–57 → 54–55/72–73 → 70–71/88–89 → 86–87)	Three point transposition: 56–57 to position 54–55; 72–73 to position 70–71; 88–89 to position 86–87	Alteration of repetitive WGQP motif through a three point separation of WG and QP, achieved through transposition of WG	Figures S6C and S8C
PrP W → A 50–90	Five point tryptophan to alanine mutation at positions 56, 64, 72, 80, 88	Reduction of interaction with plasma membrane	Figures S6C and S8C
PrP H → A 50–90	Four point histidine to alanine mutation at positions 60, 68, 76, 84	Inhibition of copper binding	Figures S6C and S8C
PrP K → A 94–110	Four point lysine to alanine mutation at positions 100, 103, 105 and 109	Reduced positive charge of CC2	Figures S6D and S8D
PrP P → A 94–110	Two point mutation at position 101 and 104	Altered SH3 binding site	Figures S6D and S8D
PrP V → A 111–134	Three point mutation valine to alanine at positions 111, 121 and 122	Prion protein with increased hydrophobicity	Figures S6D and S8D

This toxic function of GDL requires the induction of an intramolecular R28-H140 hydrogen bond [16]. Because their toxicity is rapid and the structural details of their interaction with PrP^C are atomistically understood, these ligands represent useful tools in the investigation of prion-initiated neurodegeneration [17], and have enabled the identification of the FT as the mediator of neurotoxicity [10].

The FT can be dissected into distinct domains: a polybasic region (PR: residues 23–31) encompassing an N-proximal charge cluster (CC1: residues 23–27), a region preceding the octapeptide repeat region (pre-OR: residues 28–49), the five octapeptide repeats (OR: residues 50–90), a second charge cluster (CC2) and a hydrophobic core (HC: residues 111–134) [18]. These structural domains play distinct roles in PrP^C-mediated neurotoxicity, as shown by the

differential patterns of prion-associated degeneration in mice expressing the cognate deletion mutants of PrP^C [18].

Here we have perturbed the sequence of the FT in order to delineate the requirements for neurotoxicity. Using AAV-mediated expression of NG and various PrP^C mutants in cerebellar organotypic slice cultures (COCS), we have assessed the toxicity of 19 individual

PrP^C mutants (Table 1 and Figure 1A). We identified a lysine residue at position 27 of the *Prnp* reading frame as essential for the neurodegeneration induced by globular domain ligands (GDL). Furthermore, we found that co-expression of a PrP^C variant with an uncharged CC1 suppresses the neurodegeneration induced by toxic PrP^C from which the HC was deleted.

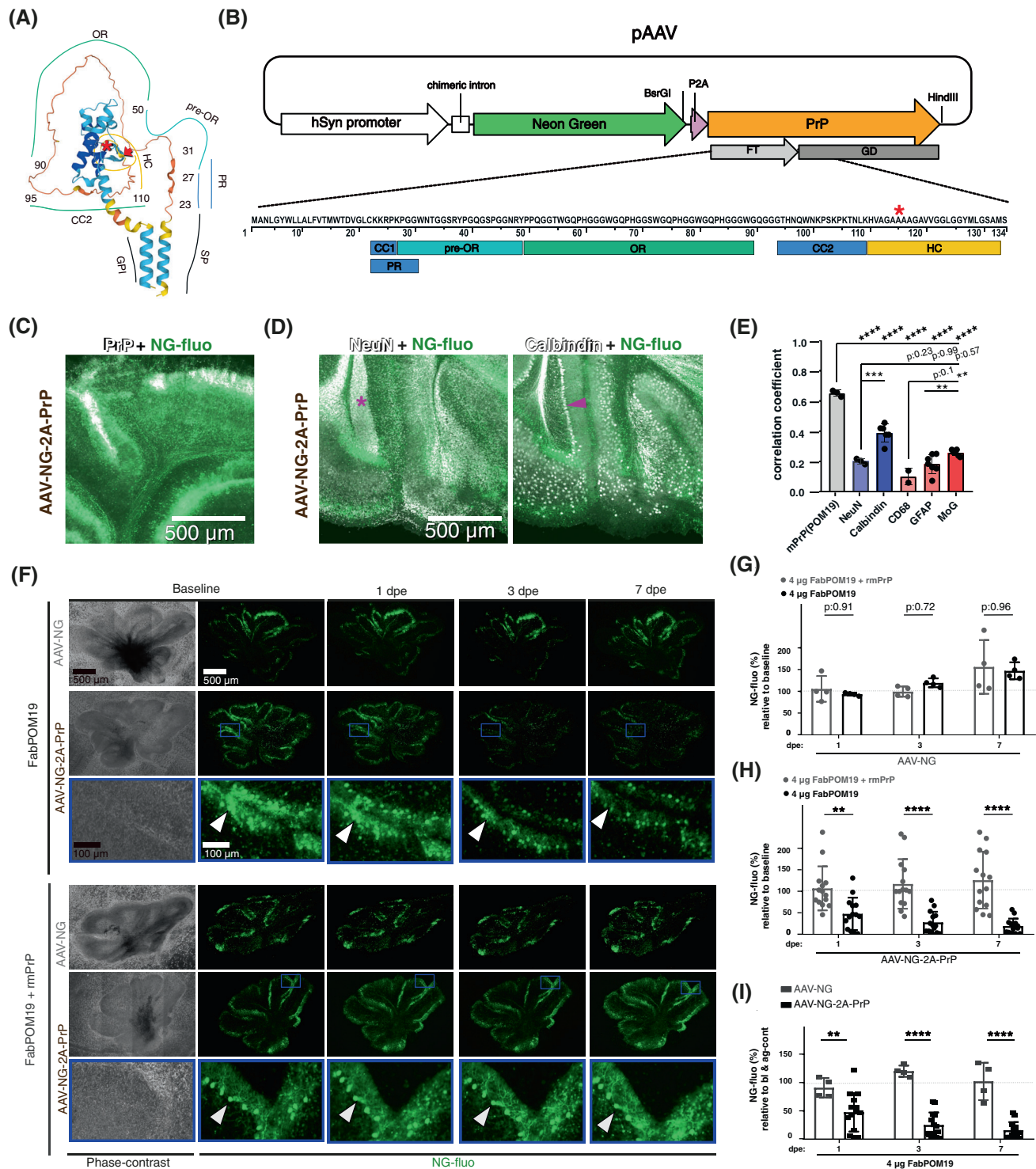


FIGURE 1 Legend on next page.

2 | RESULTS

2.1 | An ex vivo assay for probing domains of PrP relevant to neurodegeneration

To investigate the role of the different domains of the FT of PrP^C in neurotoxicity, we measured the damage to COCS expressing various PrP variants after exposure to GDLs. To assess the progressive disappearance of cells in organotypic slices reliably, we established a system for simultaneous transduction of PrP^C mutants along with the genetically encoded fluorescent marker, Neon Green (NG). We reasoned that the progressive disappearance of NG fluorescence over time would point to the degeneration of the respective cells. We thus assembled a polyprotein gene consisting of various mutants of the murine *Prnp* gene (encoding PrP^C) followed by a P2A self-cleaving sequence and NG. This transgenic cassette was placed under the transcriptional control of the neuron-specific human synapsin 1 (hSyn1) [21] promoter (Figure 1B and S1A). We transduced this construct using adeno-associated viral AAV2/6 (AAV6 capsid with AAV2 inverted terminal repeats) vectors in COCS from PrP-deficient mice (*Prnp*^{ZH3/ZH3}, [22]) and found conspicuous NG expression in Purkinje cells as expected from this particular AAV serotype (Figure 1C–E and S1B–E). To a lesser extent, NG expression colocalized with granule cells, oligodendrocytes and astrocytes (Figure 1E).

Since mice lacking PrP^C are resistant to GDL-mediated neurotoxicity [12], they provide an ideal platform for dissecting the functional domains of PrP^C by reverse genetics. We exposed transfected *Prnp*^{ZH3/ZH3} COCS (NG versus NG-2A-PrP) to chronic anti-PrP antibody treatment [12]. After 10 days of exposure to 134 nM of Fab-POM19 (which recognizes a discontinuous PrP epitope comprising residues 121–134 and 218–221 of the GD) in culture medium (5 media changes corresponding to a cumulative dose of 3.7 µg/COCS), we found that transduction restored GDL-mediated neurodegeneration of *Prnp*^{ZH3/ZH3} COCS. Conversely, slices transduced with an empty AAV vector (AAV-NG) were resistant to GDLs (Figure S2A–D).

To accelerate, challenge and validate our experimental system, we added 4 µg of the GDL Fab-POM19 in the form of directly trickled drops (henceforth called “pulse treatment”) on *Prnp*-overexpressing *iga20* COCS, and performed analyses at various time points after exposure. As expected, we observed a severe loss of neuronal nuclear antigen (NeuN, Figure S3A–D) within 24 h by both Western blotting as well as increased propidium iodide (PI) staining, a marker of cell membrane damage (Figure S3E–G).

In order to optimize the imaging and quantification of NG expression, we cultured the slices directly on coverslips which were placed into roller tubes [23]. We transduced PrP^C into COCS using AAV vectors (AAV-NG-2A-PrPwt), performed baseline confocal imaging (19 days

FIGURE 1 GDL-induced Purkinje cell degeneration in *Prnp*^{ZH3/ZH3} COCS transduced with PrP^C. (A) Structure of the full-length murine prion protein, as visualized by AlphaFold [19, 20]. The numbers indicate residue positions. SP: signalling peptide. GPI: glycosylphosphatidylinositol anchor. CC1: charge cluster 1. PR: polybasic region. Pre-OR: region preceding the octapeptide repeats (OR). CC2: charge cluster 2. HC: hydrophobic core. The red asterisk denotes the border between the flexible tail (FT) and the globular domain (GD) at residue 123/124. Red arrowhead: residue 134. (B) Schema of the polyprotein vector. A P2A self-cleavage site enables the coordinated expression of NeonGreen (NG) and the murine wt or mutated prion protein (PrP) driven by the human synapsin 1 (hSyn1) promoter. The replacement of wt *Prnp* with cassettes encoding mutated *Prnp* versions was performed using the BsrGI and HindIII restriction sites. FT: light grey. GD: dark grey. Red asterisk: border between FT and GD. Coloured blocks illustrate the different domains of the FT. Light blue: CC1 and CC2; turquoise: pre-OR; green: OR; orange: HC. (C, D) Representative micrographs of cerebellar organotypic slice cultures (COCS) 19 days post transduction with AAV-hSyn1-NG-2A-PrP. (C) Immunofluorescence staining for PrP with POM19 (white) demonstrates a high correlation of expression. Green: fluorescent signal for Neon Green. (D) Co-immunostaining for neuronal protein markers localizes NG-fluorescence expression predominantly to Purkinje cells (magenta arrowhead) rather than to granule cells (magenta asterisk). Neuronal nuclear antigen (NeuN, left panel, in white) expressed in cerebellar granule cells and Calbindin (right panel, white) expressed in Purkinje cells. Green fluorescence signal: NeonGreen. (E) Immunofluorescence colocalisation analysis (Pearson’s coefficient) of different markers with NG-fluo. Representative images of this analysis are shown in C, D and in S1 B–E. The NeonGreen signal is highly correlated with POM19 staining (PrP) and with calbindin. Blue bars: Neuronal markers (NeuN and calbindin). Red bars: non-neuronal markers: CD68 (microglia), glial fibrillary acidic protein (GFAP, expressed by astrocytes) and myelin-oligodendrocyte glycoprotein (MoG, expressed by oligodendrocytes). Each dot represents one COCS, mean ± SD; ***p* < 0.01; ****p* < 0.001; *****p* < 0.0001. Two-way ANOVA, Tukey post hoc test. (F) Phase-contrast (left) and fluorescence micrographs (right) of *Prnp*^{ZH3/ZH3} COCS 2 weeks after transduction with AAV-hSyn1-NG-2A-PrP or AAV-hSyn1-NG (10⁹ TU/ml, leftmost column), and at various time points after a pulse of FabPOM19 (4 µg in 10 µl PBS). NG expression by Purkinje cells was initially conspicuous but became gradually reduced under FabPOM19 treatment, and was drastically reduced after 1 week. Pre-incubation of FabPOM19 with a 3 × molar excess of PrP^C (lower three rows) prevented the disappearance of NG fluorescence. Blue rectangles: magnified regions. White arrowhead: bodies of individual Purkinje cells. (G) NeonGreen (NG) morphometric analysis (details: Figure S4) revealed no significant degeneration of NG-only expressing COCS treated with FabPOM19. Data points: percentage of NG expression at baseline. AAV titre: 10⁹ TU/ml; each dot represent one COCS, mean ± SD, two-way ANOVA, Sidak post hoc test. Dpe: Days post exposure to FabPOM19 or blocked control. (H) Progressive, massive decrease in NG expression over time (24 h, 72 h, 1 week) in slices infected with AAV-Syn-NG-2A-PrP and subjected to FabPOM19 treatment. AAV titre: 10⁹ TU/ml. Each dot represents one COCS. Mean ± SD, two-way ANOVA, Sidak post hoc test; ns = not significant, *****p* < 0.0001, two-way ANOVA, Sidak post hoc test. Dpe: Days post exposure. (I) Data points from G and H additionally divided by the average NG expression of COCS treated with a blocked antibody at the same time point. The data representation used in this figure for the neurodegeneration assay is also used in the following figures. Each dot represents one COCS, mean ± SD, ns = not significant, **p* < 0.05, ***p* < 0.01, *****p* < 0.0001 one-way ANOVA, Sidak post hoc test. Dpe: Days post exposure

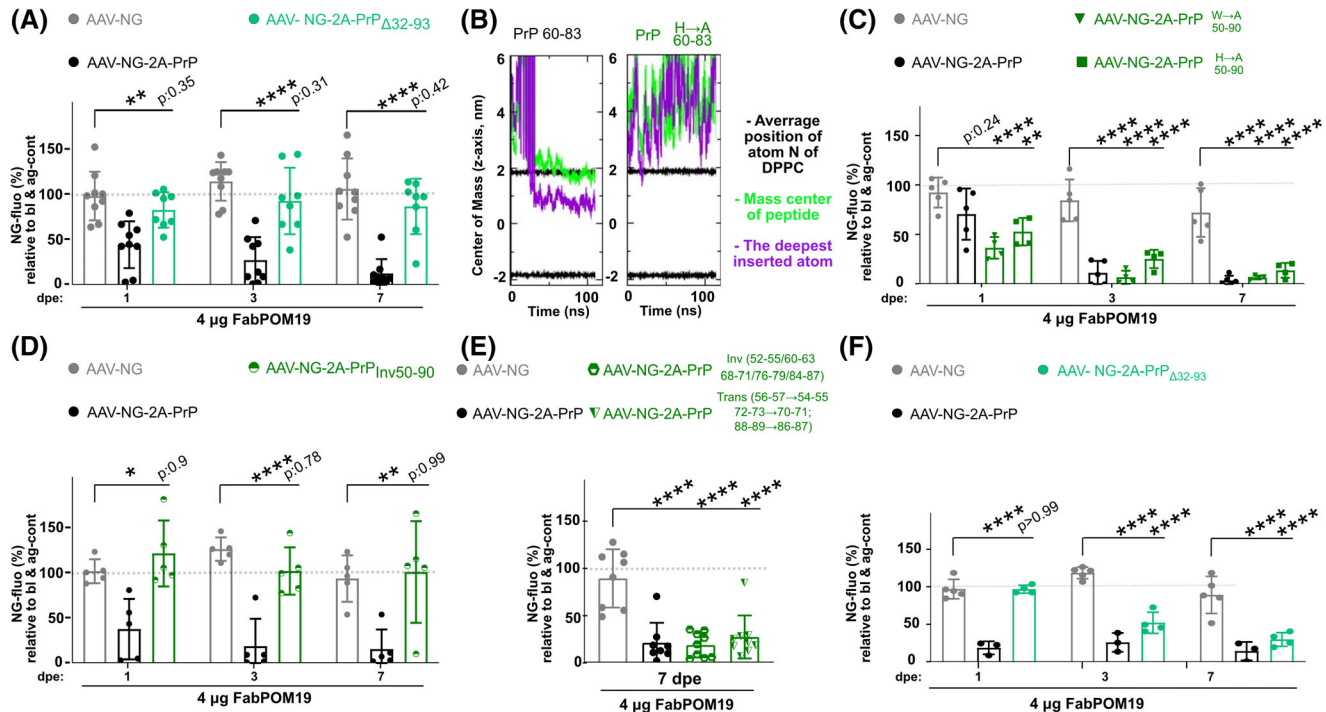


FIGURE 2 The OR modulates GDL-mediated neurodegeneration but is not essential. (A) Morphometric NG time-course analysis showing that PrP^C but not PrP Δ 32–93 restores GDL-induced neurodegeneration in *Prnp*^{ZH3/ZH3} COCS. AAV titre: 1 E+9 TU/ml. Here and in all following panels if not otherwise specified: Each dot represents one COCS, **p* < 0.05, ***p* < 0.01, ****p* < 0.001, *****p* < 0.0001; each data point in percentage of NG expression at baseline is divided by the average NG expression of COCS treated with blocked antibody at the same time point; one-Way ANOVA, Sidak post hoc test. Dpe: days post exposure. (B) Molecular dynamics simulation of the PrP60–83 peptide with a three-point tryptophan to alanine mutant (right) showed no insertion of the FT into the plasma membrane in contrast to wt PrP60–83 (left). Further details on this experiment are given in Figure S7. (C, D) Time course analysis demonstrates full restoration of neurodegeneration involving PrPW→A 50–90 and PrPH→A 50–90 mutants (C), but not PrPInv(50–90) with an inversed OR sequence (D). (E) Neither a flip of components of the OR PrPInv(52–55/60–63/68–71/76–79/84–87) nor a three-point transposition of tryptophan-glycine elements PrPTrans(56–57 → 54–55/72–73 → 70–71/88–89 → 86–87) blocks FabPOM19 mediated neurodegeneration. One-way ANOVA, Dunnett’s post hoc test. (F) Repetition of the experiment performed in B, but with COCS exposed to a 10-fold higher AAV titre, resulting in approximately 3-fold higher expression (Figure S9A) and faster kinetic of NG loss. COCS expressing PrP Δ 32–93 remained intact after 1 day of FabPOM19 exposure, but experienced severe neurodegeneration at later time points

post transduction) at 5 different depths, and generated maximal-intensity projections (Figure S4A–B) followed by NG morphometry (Figure S4C–E). With this method, NG expression was stable for ≥ 4 weeks post transduction (Figure S4F–G). Immediately after baseline scanning, we pulse-treated each COCS with 4 μ g of FabPOM19 or, for control, FabPOM19 inactivated by preincubation with its cognate antigen. Then, we reimaged COCS in a time-course experiment at 1, 3 and 7 days post exposure (dpe) to treatment using identical confocal imaging settings as for baseline imaging, and compared NG expression of each COCS and at each time-point with its baseline expression. Loss of NG expression, indicating incipient neurodegeneration, was found already at 1 dpe, with increasing severity at 3 and 7 dpe (Figure 1F–I), and a trend toward increased PI incorporation by NG-expressing Purkinje cells (*p* = 0.1), corroborating the suggestion that NG loss was the result of cell death (Figure S5A–B). We obtained similar results when repeating this experiment with a different neurotoxic GDL (FabPOM1; binding residues: 138–147; 204; 208; 212) (Figure S5C).

2.2 | Role of the octarepeats in anti-PrP antibody mediated neurodegeneration

Mice overexpressing PrP Δ 32–93 are resistant to toxic GDLs [12]. Accordingly, we found no significant reduction of NG expression (*p* = 0.42 at 7 days post exposure) when COCS were treated with toxic GDLs 2 weeks after transduction with AAV-NG-2A-PrP Δ 32–93 (Figure 2A, Table 1) despite intact surface expression of the mutant protein (Figure S6C). The FT may exert its toxic function via a pathological interaction with membrane constituents [24]. The OR features a high tryptophan content which may favour its insertion into biological membranes [25], suggesting that the FT may exert its pathological function by integrating the OR into the plasma membrane. We examined this possibility using molecular dynamics (MD) simulations (Figure S7A). We found that a potential OR insertion into the membrane can occur spontaneously within a 100-ns time scale simulated for the PrP60–83 peptide (Figure S7B), respectively within 50-ns for the PrP21–90 peptide (Figure S7C). Furthermore, a three-

time tryptophan-to-alanine mutation in the PrP60–83 peptide would block this interaction (Figure 2B, Figure S7D). In order to test this observation experimentally, we transduced into *Prnp*^{ZH3/ZH3} COCS a *Prnp* mutant in which all tryptophan residues in the OR region were replaced with alanines (Table 1). The protein expression levels of the mutant were similar to those of wt PrP^C (Figure S9A). This manipulation was expected to prevent any insertion events (Figure 2B). However, we found that the tryptophan-mutated construct restored GDL-mediated neurodegeneration (Figure 2C). This makes the membrane-insertion hypothesis of GDL-mediated neurodegeneration unlikely. Recent reports suggest that the neurotoxic activity of the FT is inhibited by a copper-mediated *cis* interaction with the GD [26, 27]. If so, the four histidine residues in the OR, which bind Cu²⁺ with sub-nanomolar affinity [28], would be essential for this phenomenon. To test the influence of these residues on GD-ligand mediated neurodegeneration, we replaced all four histidines in the OR with alanines (Table 1). However, we did not detect any reduction of GDL-induced neurodegeneration in comparison to wt PrP (Figure 2C). The distance between the two charge clusters in the PrPΔ32–93 deletion mutants was reduced, with possible secondary effects on protein function that may not be directly linked to the OR. We generated a construct with an entirely inverted OR (Table 1), which was expected to show similar physical properties as wt PrP^C but altered interaction capabilities with ionic or proteinaceous binding partners. Protein surface expression and glycosylation of the mutant were intact (Figure S6C, Figure S8C). Interestingly, this construct did not restore GDL-induced neurodegeneration (Figure 2D). In an attempt to narrow down the critical amino acid motifs in the OR more precisely, we designed two additional PrP^C mutants based on the same concept but with smaller modifications. On one hand, we generated a construct in which the repetitive WGQP motifs are intact but the stretches in-between are inverted and on the other hand, we modified exactly this motif at three positions by translocation of WQ (Table 1). As both mutations restored GDL-mediated neurodegeneration (Figure 2E), this approach was not successful in the further identification of OR amino-acid motifs important for mediating neurodegeneration. Since GDL-mediated neurodegeneration is dependent on PrP^C expression levels [12], we asked whether PrPΔ32–93 might mediate neurodegeneration if more strongly overexpressed in Purkinje cells. Indeed, at a threefold higher expression level than assessed previously (Figure S9A), PrPΔ32–93 restored GDL-mediated neurodegeneration (Figure 2F). In contrast to wt PrP expressed at a comparably high level, the induction of degeneration was delayed by 1 day. This finding suggests that the OR is an important, but not essential, modulator of anti-prion GDL-mediated neurodegeneration.

2.3 | A lysine residue at position 27 is essential for PrP^C mediated neurodegeneration

We then systematically analysed various mutants of PrP^C carrying deletions in each of its functional units (Table 1). To robustly identify the most relevant regions for GD mediated neurodegeneration, COCS were infected with a five-fold higher functional titre than used in our previous experiments. This resulted in two-fold higher PrP expression level (Figure S9B). We found that all constructs, except those lacking the PR (PrPΔ23–31), were able to restore GDL-mediated neurodegeneration (Figure 3A). However, all mutants showed a one-day delay in the velocity of induction. In addition, PrPΔ111–134 showed low expression in CAD5 cells (Figure S8A) and no expression in COCS (Figure S9B), probably recapitulating the previously described phenotype of mice expressing deletion mutants of PrP in this region [29]. We excluded this construct from further analyses.

Electrophysiological assays in cells had established the importance of the PR as the main effector of a GDL-mediated (POM1, POM11, D18) pathological inward current, as well as the importance of positively charged amino acids within this domain for triggering spontaneous currents in cells expressing PrP^C with a deletion in the central domain (PrPΔ105–125) [13]. We therefore asked whether these charged amino acids are equally important for GDL-mediated neurodegeneration in COCS. We mutated the three lysine residues of the CC1 to alanine (Table 1). As with the polycationic region-depleted mutant, PrPK→A 23–27 did not restore anti-prion antibody-mediated neurodegeneration (Figure 3B,C). In order to establish whether all lysine residues are equally important, we compared a construct with lysine-to-alanine conversions of the first two N-terminal lysines [17, 30] to conversion of lysine at position 27 (Table 1). Surprisingly, the point mutation of lysine 27 proved sufficient to block GDL toxicity, probed with FabPOM1 and FabPOM19 (Figure 3B,C), whereas PrPK→A 23–24 fully restored GDL-mediated neurodegeneration. Protein expression levels were similar for all constructs (Figure 3D). We then asked whether the effect is charge-dependent by expressing a PrPK→R 23–27 construct (Table 1). This construct restored GDL-mediated neurodegeneration (Figure 3B,C). In line with these data, we found that the CC1 ligand Fab83, which interacts with the three N-terminal lysines, is neuroprotective in prion-infected COCS [31]. We therefore used ELISA to investigate the binding capacity of Fab83 to the protein mutants PrPK→A 23–24 versus PrPK→A27 and found a similar binding reduction (Figure 3E).

2.4 | CC2 ligand neurotoxicity is CC1 dependent

Analogously to previous studies [12], deletion of CC2 had no effect on GDL-mediated neurodegeneration

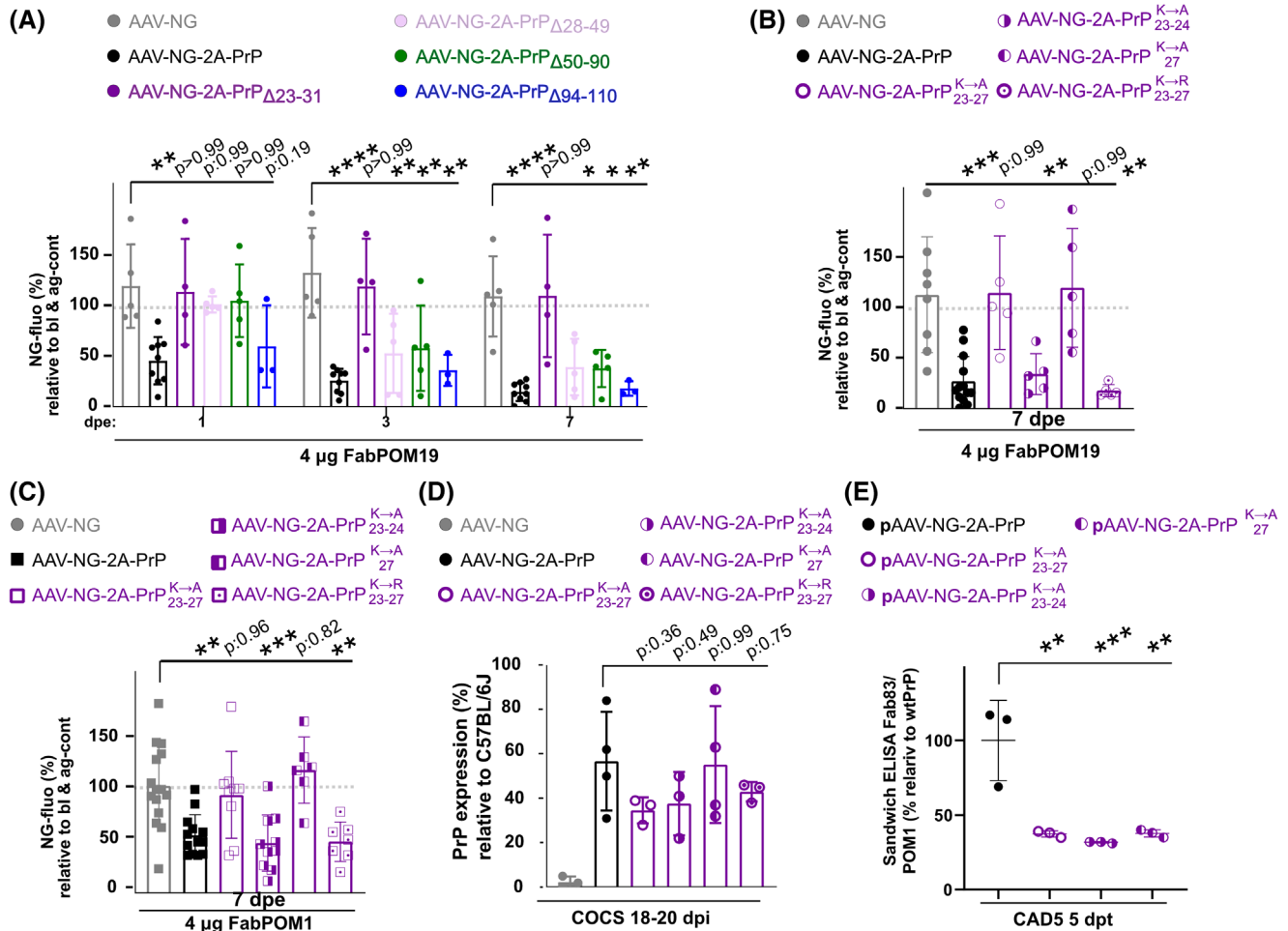


FIGURE 3 A LYS₂₇ → ALA point mutation suppresses GDL-mediated neurodegeneration. (A) Time-dependent FabPOM19-induced neurodegeneration in COCS expressing various *Prnp* deletion mutants. All mutants except those with a deletion of the polybasic region (violet) restored FabPOM19 toxicity. Here and henceforth: AAV titre 5 E+9 TU/ml, each dot represent one COCS, * $p < 0.05$, ** $p < 0.01$, *** $p < 0.001$, **** $p < 0.0001$. One-way ANOVA, Sidak post hoc test. Datapoints: percentage of NG expression at baseline divided by the average NG expression of COCS treated with paratope-blocked antibody at the same time point. (B) Prion protein mutants with all K → A mutations within the polybasic region, or with K → A only at position 27, do not restore anti-prion antibody mediated neurodegeneration induced by FabPOM19. In contrast, replacing the lysines at position 23 and 24 with alanines did not modify FabPOM19 toxicity. K → R point mutations had no impact on FabPOM19 toxicity. (C) The experiment shown in B was replicated with the toxic GDL FabPOM1. (D) PrP^C expression level from COCS transfected together with those used for the experiments in B and C but grown separately on an inlay demonstrate similar expression levels of wt versus CC1 mutant PrP. Expression levels shown are relative to PrP^C expression levels of cerebellar homogenate from C57BL/6J wt mice. Sandwich ELISA (coating: POM1; probing biotinylated POM19). One dot represents one inlay with 11 slices. (E) ELISA (Coating with Fab83, incubating with wt or altered PrP^C, and probing with biotinylated FabPOM1) assessing the binding capacity of Fab83 to the three CC1-mutated PrP^C versions. Mutation of K23 and K24 had a similar effect as the single-point mutation of K27. All concentrations relative to wtPrP^C 5 days after transduction of CAD5 cells with pAAV vectors. ELISA data were performed in triplicate. ** $p < 0.01$, *** $p < 0.001$

(Figure 3A). Moreover, PrP^C mutants with a deionized CC2 or with an altered Src homology 3 (SH3) [32] domain restored GDL-mediated neurodegeneration (Figure 4A). Several studies have reported a high-affinity interaction of the CC2 with amyloid- β (A β) oligomers [8, 33]. Additionally, PrP^C may act as a receptor for A β -oligomers mediating impairment of synaptic plasticity [7, 8].

In order to study pathological CC2 ligand interactions, we performed pulse treatment experiments with the high-affinity CC2 domain ligand D13, previously found to induce neurodegeneration with a delayed kinetic in intact mice [10]. We found significant reduction

of NG expression, detectable at significant levels after 72 h post exposure (Figure 4B), which represents a delay in contrast to GDL-mediated neurodegeneration (neurodegeneration 24 h post exposure). We then investigated the binding capacity of FabD13 to the protein mutants with an uncharged CC2 or an altered SH3 using an enzyme-linked immunoassay (ELISA) (Table 1). We found that the lysine residues in the CC2 largely impart FabD13 binding (Figure 4C). Interestingly, the SH3 mutant protein still partially mediates FabD13-induced neurodegeneration (Figure 4D,F).

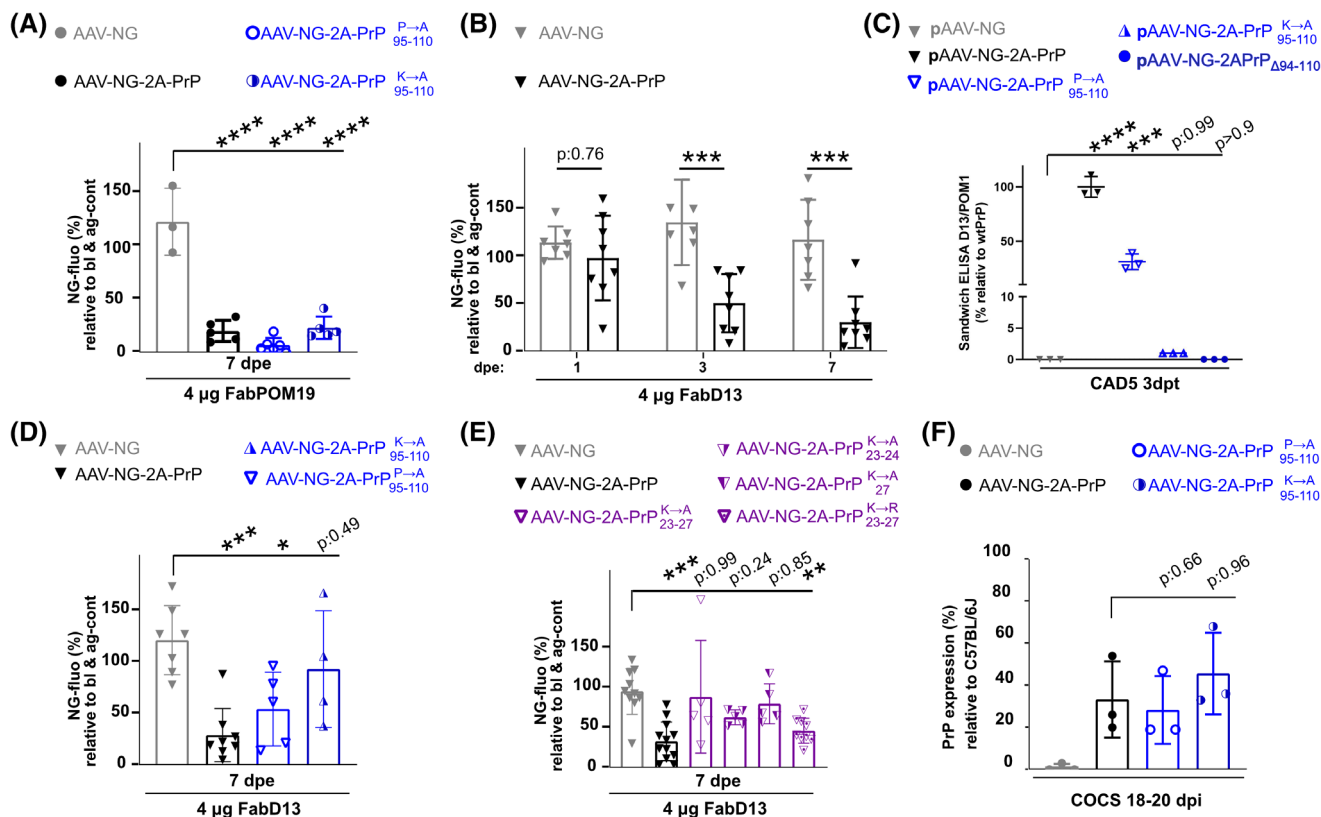


FIGURE 4 CC2-ligand mediated toxicity requires the polybasic region. (A) Expression of PrPP→A 94–110 and PrPK→A 94–110 fully restore FabPOM19 mediated neurodegeneration. Here and henceforth: AAV titre 5 E+9 TU/ml, each dot represent one COCS, * $p < 0.05$, ** $p < 0.01$, *** $p < 0.001$, **** $p < 0.0001$. One-way ANOVA, Dunnett's post hoc test. (B) CC2 ligand FabD13 induced significant neurodegeneration at 72 h and 1 week after pulse treatment of the antibody. Sidak post hoc test. (C) CAD5 cells were transduced with pAAV vectors and lysed after 3 days. Lysates were probed by D13/POM1 sandwich ELISA. We observed no binding of D13 to PrPΔ94–110 and drastically reduced binding to the uncharged CC2 PrP^C mutant PrPK→A 94–110. In contrast, PrPP→A 94–110 showed only minimally reduced binding to D13. All expression levels are relative to wtPrP^C. ELISA data were performed in triplicate. **** $p < 0.0001$. (D) Expression of PrPP→A 94–110 slightly sensitizes COCS against FabD13 mediated neurodegeneration in contrast to the expression of PrPK→A 94–110. Two-Way Dunnett's post hoc test. (E) *Prnp* variants with K → A mutations of the entire polybasic region, of K23 and K24, or of K27 (but not K → R mutations) fail to restore FabPOM19 toxicity. (F) Similar expression levels of wt and CC1-mutant PrP determined in COCS transfected together with those used for the experiments in A and D but grown separately on an inlay. Sandwich ELISA (coating: POM1; probe: biotinylated POM19). Each dot represents one inlay with 11 slices

We then asked whether the CC1 domain mediates the CC2-related toxicity in addition to GDL-induced neurodegeneration. As for GDL-mediated neurodegeneration, we found that PrPK→A 23–27 as well as PrPK→27 do not mediate FabD13-induced neurodegeneration (Figure 4E). However, in contrast to FabPOM19-induced toxicity, PrPK→A 23–24 was unable to fully rescue the toxicity induced by CC2 ligands (Figure 4E) ($p = 0.24$).

2.5 | PrP^C with an uncharged CC1 suppresses neurodegeneration induced by HC-deleted PrP^C

Expression of PrP^C with a deletion of residues 105–125, spanning six residues of the CC2 and fifteen of the HC, is known to induce spontaneous degeneration of the nervous system [13, 14]. Specifically, the brain of mice lacking the entire HC with an intact CC2 (Δ111–134) shows white-matter vacuolation and astrogliosis in the

cerebellum, brain stem and corpus callosum, without description of significant neuronal degeneration [29]. The low expression of transduced PrPΔ111–134 described above suggests a neurotoxic effect. To discriminate between defective expression of the viral vector and degenerative effects induced by PrPΔ111–134, we co-incubated slices with AAV-Syn1-NG-2A-PrPΔ111–134 and AAV-Syn1-NG with a 1:10 ratio. In contrast to co-incubation with the AAV-Syn1-NG-2A-PrP_{wt}, we found a drastic reduction of NG expression when PrPΔ111–134 was co-expressed with AAV-Syn1-NG (Figure 5A,B), suggesting neurotoxicity of the HC truncated construct. A central characteristic of this toxic deletion mutant is that the effect can be rescued by co-expression with molar excess of wt PrP^C [14, 16]. We therefore co-infected COCS with AAV-Syn1-NG-2A-PrPΔ111–134 and AAV-Syn1-NG-2A-PrP_{wt} at a 1:10 ratio and could partly rescue the degenerative effect (Figure 5A,B).

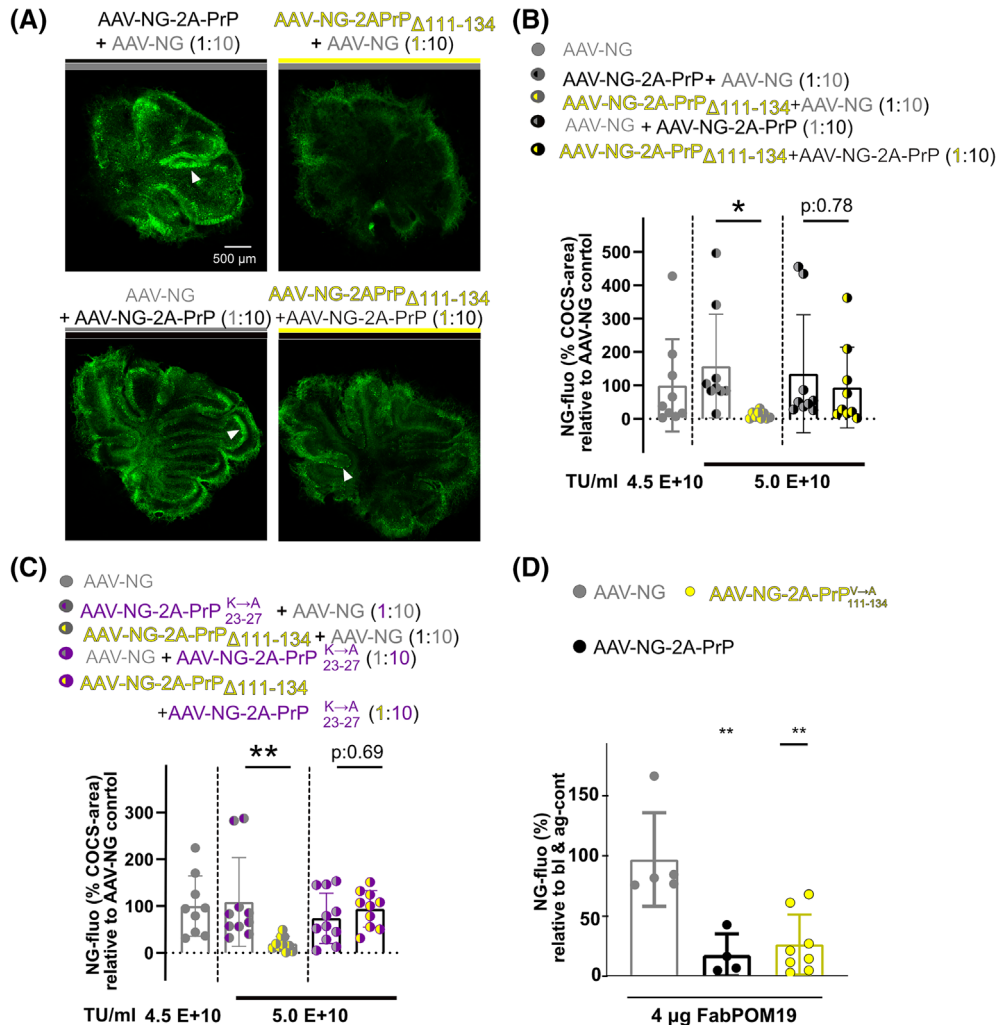


FIGURE 5 Co-expression of wt PrP counteracts the degeneration induced by PrP Δ 111–133. (A) Representative micrographs of COCS 2 weeks after co-transduction with various combinations of AAV vectors. Co-transduction with 10:1 or 10:1 AAV-hSyn1-NG (4.5 E+10 TU/ml) + AAV-hSyn1-NG-2A-PrP (4.5 E+9 TU/ml) (left column) did not impair Purkinje cell viability. In contrast, co-expression of AAV-hSyn1-NG-2A-PrP Δ 111–134 AAV-hSyn1-NG (1:10) resulted in decreased NG expression and drastic reduction of Purkinje cell labelling (upper right). This effect was partially mitigated by coexpressing AAV-hSyn1-NG-2A-PrP Δ 111–134 + AAV-hSyn1-NG-2A-PrP (1:10; lower left). White arrowhead: NG-labelled Purkinje cell layer. (B) Quantification of NG expression from the experiments shown in panel A. First column NG expression after incubation 4.5 E+10 TU/ml of AAV-hSyn1-NG alone. Here and henceforth: graphs show percentage of NG⁺ pixels within COCS, divided by COCS infected with AAV-hSyn1-NG. Each dot represents one COCS, * p < 0.05, ** p < 0.01, *** p < 0.001, **** p < 0.0001. Two-way ANOVA, Sidak post hoc test. (C) NG morphometry showing preservation of NG expression by co-expression of PrP Δ 111–134 and PrP^C mutants with uncharged CC1 (3 \times K \rightarrow A). (D) PrP mutants in which all valine residues in the HC were replaced by alanine residues restored antibody-mediated neurodegeneration. One dot represents one COCS, mean \pm SD, ns = not significant, 5 E+9 TU/ml; ** p < 0.01, one-way ANOVA, Dunnett's post hoc test

The introduction of an additional deletion in the polybasic region (residues 23–31) or a combinatorial expression with an uncharged CC1 abolishes the pathological inward current of toxic 105–125 deletion mutants in cell culture [13, 34, 35]. We therefore wondered if PrP^{K→A} 23–27 is incapable of rescuing PrP Δ 111–134 induced neurodegeneration in contrast to wt PrP. However, co-expression of PrP Δ 111–134 with PrP^{K→A} 23–27 at a 1:10 ratio fully restored NG

expression, indicating that the health of transduced neurons was rescued (Figure 5C).

The hydrophobic valine residues within the HD are contributing to the physical properties of this domain. We therefore generated a construct in which we replaced all valines between residues 111–134 with alanines (PrP^{V→A} 111–134). In COCS at 19 dpi, we found no difference in NG expression compared to AAV-Syn1-NG-2A-PrP_{wt}. In fact, this construct fully mediated neurodegeneration (Figure 5D).

3 | DISCUSSION

3.1 | A rapid ex vivo assay to study PrP-mediated neurodegeneration by reverse genetics

PrP^C can mediate neuronal cell dysfunction and death in prion infections, by way of interaction with aggregated A β , α -Synuclein and tau, and upon exposure to antiprion antibodies [7–10, 12, 13, 17]. The prevailing view is that under physiological conditions, the GD prevents pathological effects that are allosterically mediated by the FT [12, 13]. Accordingly, mice expressing an FT directly fused to the GPI anchor, but lacking the GD, develop lethal neurodegeneration [24]. Nuclear-magnetic resonance spectroscopy has revealed that the FT is entirely unstructured [3], which suggests that it may represent an optimal target for therapeutic ligands as it offers a good spacing of the amino acid residues with minimized steric effects. Data from genetically modified mice expressing PrP^C deletion mutants have provided important details about the functional domain of the FT [20]. We have now expanded this work with a reverse-genetics study addressing the role of various PrP^C domains and their composition in mediating prion-related neurodegeneration.

These studies are often performed by generating transgenic mice, which is laborious, lengthy and very costly. We have therefore developed an ex vivo method relying on AAV-mediated gene transfer of a polyprotein vector system to express PrP^C in combination with NG to cerebellar organotypic slices under the hSyn1 promoter. We expected transfected neurons to lose NG expression upon degeneration. In order to validate the predictive value of this method, we measured the effect of toxic antiprion antibodies on NG expression using calbindin morphometry and PI incorporation. Consistent with the experiment with transgenic PrP Δ 32–93, which were resistant against GDL in previous experiments, we did not observe neurodegeneration at moderate PrP Δ 32–93 expression levels (20% relative to the PrP concentration in wt brain homogenates), whereas deletion of the CC2 had no effect on GDL-mediated neurodegeneration [12]. We then proceeded to use this model system for assessing the effects of 19 different *Prnp* mutants on GDL-associated neurodegeneration.

3.2 | The OR is a non-essential but powerful amplifier of allosteric FT-dependent neurotoxicity

The OR region of PrP^C plays multiple roles in neurodegeneration. The expansion of the OR in humans results in autosomal-dominant prion disease [36]. Transgenic mice expressing constructs with expanded OR develop ataxia and cerebellar atrophy [37, 38]. Further, the OR ligand POM2 has a protective effect on GDL-induced neurodegeneration and prolongs the life of mice expressing the

neurotoxic PrP Δ 94–134 mutant [12]. Additionally, mice expressing a truncated PrP^C form encompassing the OR residues (PrP Δ 32–93) were found to be resistant to GDL-mediated neurodegeneration [12].

Here we disprove the hypothesis that the FT exerts its pathological function by integrating the OR into the plasma membrane via lysine-tryptophan residues. Histidine residues associated with copper binding are not essential for allosteric FT neurodegeneration. We further found that drastic overexpression of PrP Δ 94–134 can induce GDL-mediated neurodegeneration albeit with a slower kinetic. This finding aligns with initial results from prion inoculation studies, which showed that these mice displayed milder signs of neurodegeneration compared to wt mice. Only the motor neurons in the cervical segment of the spinal cord were found to be affected [39]. The specific vulnerability of these neurons may be tested by adapting the assays presented here to organotypic spinal-cord slice cultures [40]. Collectively, these data indicate that while the OR may not be essential, it is an important amplifier of FT-dependent neurodegeneration.

3.3 | Lysine 27: A priority target for neuroprotective compounds

In line with previous reports [13], we provide strong evidence that the polybasic region of PrP^C is the main effector domain of allosteric FT neurodegeneration. Mice expressing physiological levels of *Prnp* Δ 23–31 showed no clinical signs of disease at >400 dpi after intracerebral prion (RML) inoculation [41] and mice expressing mouse PrP with mutation in the 3 lysines of the polybasic region are highly resistant to RML and 22 L prions [42, 43]. Our study provides additional evidence that the charged lysine at position 27 has a major impact on GDL-mediated neurodegeneration. It is likely that charged lysines in the polycationic cluster mediate the inappropriate interaction with membrane constituents exerting the toxic function. Some of these mediators may be G-protein coupled receptors (GPCRs), since PrP^C was found to interact with several GPCRs including the adhesion GPCR Gpr126 [44] and the metabotropic glutamate receptors mGluR1 and mGluR5 [45]. Of note, the three lysines are conserved among prion proteins from at least 48 species, but are lacking in the prion protein encoded in turtle, chicken, frog and zebrafish [46]. The latter four species are not known to be susceptible to prion disease.

We demonstrate that CC1 ligand Fab83 [31] strongly interacts with all three lysines in the polybasic region including K27 and therefore represents an optimal compound for protection from neurodegeneration in prion disease. Surprisingly, Fab83 prevented prion-induced neurodegeneration in COCS less efficiently ($p < 0.01$) than the OR binder Fab8, Fab44, Fab71 and Fab100 ($p < 0.0001$) [31]. Treatment of prion-infected COCS with these OR binders resulted in reduced levels of the PK-

resistant scrapie isoform of PrP^C (PrP^{Sc}) in addition to neuroprotection. In contrast, Fab83 only affected neurodegeneration but not the level of PrP^{Sc}. This finding suggests the existence of additional neurodegenerative pathways beyond allosteric FT activation. In addition, it may explain why transgenic mice with *Prnp*Δ23–31 expression levels comparable to *tga20* mice overexpressing wt PrP^C became terminally ill, though with a longer latency [41]. Therefore, combining neuroprotective CC1 ligands with blockers of prion conversion might represent a rational treatment approach. Finally, blocking CC1 mediated neurodegeneration represents an interesting tool for addressing pathologic pathways independent of PrP^C.

3.4 | A charged polybasic region is essential for CC2-mediated neurodegeneration

While antibodies and antibody-derived GD ligands can induce rapid neurodegeneration, ligands that bind to the CC2 domain can also be neurotoxic [11, 12], maybe mimicking the pathologic interaction of amyloid-β with PrP^C. Here we show that, similarly to toxic GDL, this destructive interaction requires a charged polybasic region. However, in contrast to GDL-mediated neurodegeneration, all lysine residues of CC1 have an impact on the degenerative interaction. This may be due to differences in the structural rearrangement of the FT upon binding to CC2 ligands in contrast to GDLs. Indeed, CC2 binders have found to have the strongest stimulation on proteolytic shedding by ADAM10, associated with an extended N-terminal conformation [47]. This difference could also be the basis for the delayed kinetic of CC2-mediated neurodegeneration described in intact mice [10] and recapitulated here in COCS.

3.5 | A versatile model for prion-related neurodegeneration

Mice lacking the entire HC (Δ111–134) suffer from extensive white matter degeneration [14, 16]. Here we found that overexpression of PrPΔ111–134 induces degeneration of Purkinje cells, which can be rescued by co-expression of wt PrP^C. Residues 111–134 affect the α-cleavage site of PrP^C, and their deletion impairs the release of the N1 fragment [48]. There is evidence that a charged CC1 mediates the pathology caused by *Prnp* deletion mutants [13, 34, 35], suggesting similarities to GDL-mediated neurodegeneration. When co-expressed, wt PrP^C may block pathological interactions of PrPΔ111–134 with unknown partners through its CC1 lysines. However, the co-expression of PrP^C with an uncharged CC1 prevented the neurodegeneration induced by PrPΔ111–134 as well. As PrP^C is required for neuronal survival, these findings suggest that the uncharged

CC1, either as part of the full-length protein or released with the N1 fragment after α-cleavage, may act as an inverse agonist of the neurotoxic interaction with hitherto undefined partners, being able to engage with them but not to activate deleterious downstream cascades.

3.6 | Limitations and prospects of this study

Prion infection of cerebellar organotypic cultured slices has proved extremely useful for elucidating many aspects of the pathogenesis of these diseases. However, reverse-genetics studies have proved difficult since COCS are refractory to many types of genetic manipulations. In this study, we have found that the utilization of AAV vectors can enable a rapid analysis of the consequences of expression of many *Prnp* mutants. Crucially, AAV-mediated gene transduction has allowed us to perform experiments that in the past would have required the generation of transgenic mouse lines—an expensive and time-consuming procedure. Although COCS are ultimately derived from live mice, their use abides by the 3R precepts of animal experimentation (reduce, replace, refine) since it minimizes the number of animals necessary for drawing robust conclusions.

The AAV6 capsid infects preferentially cerebellar Purkinje neurons [49]. This peculiarity was advantageous for the current study since Purkinje neurons are large and aligned along a single plane. This morphology greatly facilitates the assessment of neurodegeneration. On the other hand, neurodegenerative diseases, including prion diseases, often display conspicuous selectivity in the type of affected cells. Hence, it is likely that the findings reported here might not be generalizable to all neuronal cell types. The availability of novel AAV serotypes, promoters specific for neuronal subpopulations and organotypic slice cultures from different areas of the central nervous system provides a convenient path toward modelling neurodegeneration *ex vivo*, and could be used for the study of many questions of prion science and beyond.

4 | MATERIAL AND METHODS

4.1 | Animals

All animal experiments were conducted in strict accordance with the Swiss Animal Protection law and dispositions of the Swiss Federal Office of Food Safety and Animal Welfare (BLV). Animal protocols and experiments performed in this study were reviewed and approved by the animal welfare committee of the Canton of Zurich: ZH90/2013; ZH139_16. We used the C57BL/6J inbred strain and mice from the following genotypes: Zurich III *Prnp*/(*Prnp*ZH3/ZH3) [22] and *tga20* [50].

4.2 | Cell lines and chemicals

CAD5 is a subclone of the central nervous system catecholaminergic cell line CAD [51]. Generation of the CAD5 *Prnp*^{-/-} was previously described [52]. HEK 293T was derived from ATCC. Cells were cultured in DMEM supplemented with 10% FBS, 1% GM and 1% PS at 37°C in a humidified atmosphere with 5% CO₂. All compounds were purchased from Sigma/Aldrich unless otherwise stated.

4.3 | Polyprotein vectors and adeno-associated virus (AAV) production

A polyprotein vector with a P2A sequence (GSGATNFSLKQAGDVEENPGP) was assembled using Golden Gate cloning [53]. Using the Esp3I (Thermo Scientific) enzyme, the sequence of the NG (mNG) fluorophore, P2A sequence and murine wt PrP^C were assembled into the pCAG-T7 Golden Gate assembly destination vector (pCAG-TALEN-Destination, a generous gift from Dr. Pawel Pelczar). The NG-P2A-PrP^C cassette was then subcloned into adeno-associated virus (ssAAV) vector backbones with AAV2 inverted terminal repeats (ITRs), kindly provided by Bernhard Schneider (EPFL, Switzerland). In this vector, the expression of the cassette is driven by the human Synapsin I (hSyn1) promoter. All further vectors for the expression of mutant PrP^C were produced by cloning a synthetic gene block (gBlock, IDT, full sequence deposited on FigShare, <https://doi.org/10.6084/m9.figshare.c.5893787.v3>) between the BsrGI and HindIII site of the vector replacing the wt PrP^C sequence.

Viral vectors and viral vector plasmids were produced as hybrid AAV2/6 (AAV6 capsid with AAV2 ITRs), contributed by Bernhard Schneider (EPFL, Switzerland) and the Viral Vector Facility (VVF) of the Neuroscience Center Zurich (Zentrum für Neurowissenschaften Zürich, ZNZ, Switzerland). The identity of the packaged genomes was confirmed by Sanger DNA-sequencing (identity check).

4.4 | Determination of the functional AAV titre

The functional (infectious) titre in transduction units (TU/ml) was determined by qPCR after S1 nuclear digestion [54]. Viral titration was performed in HEK 293T cells. As a reference, additional HEK 293T cells were infected with an AAV-cmv-eGFP-WRPE virus with a known titre established by flow cytometry (kindly provided by Bernhard Schneider, EPFL). DNA was extracted from the cell homogenate using a NucleoSpin tissue mini kit (Macher-Nagel; ref 740952.5) following the manufacturer's instructions. After S1 nuclear

digestion (Promega, M5761), qPCR was performed for the woodchuck hepatitis virus post-transcriptional regulatory element (WRPE, forward primer: CCG TTG TCA GGC AAC GTG; reverse primer: AGC TGA CAG GTG GTG GCA AT) and albumin (forward primer: TGA AAC ATA CGT TCC CAA AGA GTT T; reverse primer: CTC TCC TTC TCA GAA AGT GTG CAT AT) including standards with a known concentration for WPRE and human albumin. Based on these standards, the viral DNA copy number per cell was established by dividing copy number WRPE over the copy number for albumin. Finally, TU/ml was established by linear regression and correlated with the reference virus.

4.5 | Antibodies and recombinant PrP generation

POM [55] and D13 [56] mouse monoclonal antibodies were produced using the hybridoma technology. Purification was performed by affinity chromatography using protein G sepharose, diluted in PBS. Antibody purity was assessed with silver-stained SDS-PAGE gels. Recombinant mouse PrP derived from E. Coli was purified by affinity chromatography, oxidized on-column and then refolded into the native state [57]. F(ab) POM fragments were generated in-house from the POM antibodies using papain digestion and purified with Protein A agarose, followed by size exclusion chromatography.

For staining and Western blotting, we purchased the following primary antibodies: Anti Calbindin rabbit (Abcam Ab25085, immunostaining 1:500); Anti Myelin oligodendrocyte glycoprotein antibody (Abcam, MOG, Ab32760, immunostaining 1:200); Anti Neuronal Nuclear antibody (Millipore, NeuN, A60, immunostaining 1:500 and Cellsignal, D3S3I, Western blotting 1:500); Anti glial fibrillary acid protein (Abcam, GFAP, Dako Z0334 1:1000); Anti CD68 (Biorad MCA1957, immunostaining 1:500); Anti GR778/BIP (Abcam, immunostaining 1:500); anti- α -GAPDH (Sigma-Aldrich, 1:15,000). The following secondary antibodies: Alexa 546 goat anti-mouse; Alexa 647 goat anti-rabbit, Alexa 594 goat anti-rat (all Biolegend, 1:1000), and horseradish peroxidase (HRP)-goat anti-rabbit IgG1 (1:10,000, Zymed) were used for staining and western blotting.

4.6 | Lipofection of cells

CAD5 *Prnp*^{-/-} cells were cultured in a 12-well format on gelatin coated (2% Gelatin) coverslips or in 6-well plates until they reached approximately 90% confluence. Cells were then transfected with the plasmid using Lipofectamine[®] 2000 (Invitrogen) according to manufacturer's instructions.

4.7 | Immunohistochemical staining of cells

Cells grown on cover slips were fixed in 4% paraformaldehyde, then incubated for 10 min in TritonX solution (0.1% in 0.5% bovine serum albumin dissolved in PBS) and blocked with 0.5% bovine serum albumin for 45 min. The cells were incubated with primary antibody (POM19: 2 $\mu\text{g ml}^{-1}$; BIP 1:500) and diluted in PBS containing 0.5% bovine serum albumin for 1 h. After washing, the cells were incubated with a fluorescent-labelled secondary antibody (Alexa Fluor 546 anti-mouse and Alexa Fluor 647 anti-rabbit; 1 $\mu\text{g ml}^{-1}$). In the last PBS wash, 4,6-diamidino-2-phenylindole, dihydrochloride (DAPI; Molecular Probes) was added and sections were mounted with Fluor Save (Calbiochem). For analysis, images were acquired with a FluoView[®] FV10i Confocal Laser Scanning System.

4.8 | Production, AAV transduction and culturing of cerebellar organotypic slice cultures (COCS)

Cultured Organotypic Cerebellar Slices (COCS) from *Prnp*^{ZH3/ZH3} and *tga20* mice were obtained as previously published [58]. 350 μm thick COCS were prepared from 9 to 12 day-old pups. After preparation, COCS were infected with AAV on a free-floating section directly after production on day 0. 21. COCS were incubated in a 6-well plate with AAV at a final concentration between 1 E+9 and 1 E+10 (as specified in the figure legend) TU/ml diluted in physiological Grey's balanced salt solution for 1 h at 4°C on a shaker.

From every incubation, 11 COCS were placed and cultured on a Millicel-CM Biopore PTFE membrane insert (6-well inserts, Millipore) in order to determine the PrP^C expression level based on a sandwich enzyme linked immunoabsorbent assay (ELISA; see below). The remaining 10 COCS were placed on cover slips and cultured in roller tubes following the published protocol [23]. In brief, coverslips were surface coated with poly-D-lysine (30,000–70,000 mol, Sigma) solution overnight. Following the addition of 30- μl of 100 U/ml thrombin (Merck) in Grey's BSS to coagulate the plasma by stirring with a pipette tip, COCS were then placed in a 20- μl drop of chicken plasma (Cocalico). The clot was allowed to dry for 3–5 min. Coverslips were then placed in a screw-top, flat-sided culture tube containing 750 μl of culture media. Subsequently, the tubes were placed in a roller drum-housed incubator at 36°C with 10 revolutions/h to allow proper aeration and feeding. The roller drum was tilted at 5° to ensure that slices received the medium during half of each rotation.

4.9 | Anti-prion antibody treatment, imaging and quantification of COCS cultured on cover slips

After 19 ± 5 days in culture, COCS cultured on cover slips were scanned using the Olympus FLUOVIEW FV1000 confocal laser scanning microscope. Three slices were scanned at the same time. Coverslips were removed from the roller tube using a Fine Point High Precision Forceps (Fisherbrand[™]) and then placed in a petri dish with a glass bottom and support with a drop of PBS. Slices were scanned at the following properties: Z moving range: –100 to 2800, enabling overlap stage position, upper (–400, 500) AR searching range, high speed (256 \times 256) map image resolution for each area, 0.17 mm of correcting ring at 38°C. Using the Z-stack multi area, 5 images per slices were taken at +50, 25, –50 (see also Figure S4). The confocal aperture was set at $\times 5$ and the laser was set at 10% with a fix sensitivity (regularly at 43%) over the whole experiment, in dependence of the mNG fluorescence expression level. From the five stack images, maximal intensity projections were generated using Fiji and images were converted into grey-scale images. Using the image analysis software “cell^P” (Olympus) the region of interest (ROI) and the COCS area were drawn in the overlay. Within this ROI percentage of NG expression (percentage of pixel) was determined with identical greyscale threshold setting for identifying positive pixels.

After baseline imaging, 4 μg of Fab fragments of anti-prion antibodies or 4 μg of Fab fragment of anti-prion antibodies pre-incubated with a three-molar excess of recombinant PrP^C in 10 μl of PBS were directly dropped on the slices. Imaging with FluoView was repeated (24 h, 72 h) 1-week after exposure to the antibody. The expression level was then calculated in relation to baseline expression.

4.10 | Generation of homogenate from CAD5 culture or COCS for protein analysis

To produce the homogenate, 100 μl of Complete[™] Mini EDTA-free Protease Inhibitor Cocktail (Sigma–Aldrich) were added to 800 μl of Lysis Buffer pH 7.5 (RIPA buffer). CAD5 cells grown in a 6-well plate were washed with PBS, scraped from the plate and aspirated in PBS solution. After centrifugation, homogenization was performed by adding lysis buffer as well as physical lysis with an 18-gauge syringe. COCS grown on PTFE Millicells inserts were washed twice in PBS and scraped off the PTFE membranes with PBS. Homogenization was performed with a TissueLyser LT (Qiagen) for 2 min at 50 Hz in lysis buffer. Bicinchoninic acid assay (Pierce[™] BCA protein assay kit, Thermo Fisher Scientific) was used to determine protein concentrations.

4.11 | Protein analysis (ELISA and Western blotting)

The enzyme linked immunoabsorbent assay (ELISA) was modified from a previously established protocol [55, 59] to a sandwich ELISA protocol for PrP^C detection in 384 well plates. All washing, aspirating and dispensing steps were performed with the BioTek Washer EL406 and MultiFlo FX. Plates were coated at 4°C overnight with 0.4 ng/μl POM1 (or 7.5 ng/μl Fab83 in SFig.11H or 0.4 ng/μl D13 in SFig.12H) in sodium carbonate and were washed 5 times with PBS containing 0.1% (vol/vol) Tween-20 (PBS-T) the next morning. Subsequently, they were blocked with 5% SureBlock™ (LuBioScience GmbH) in PBS-T and then incubated for 2 h at 25 °C. In the next step, the blocking solution was aspirated and the plates were incubated again for 2 h at 25°C with 20 μl of either rmPrP23–231 or 2-fold serially diluted slices homogenate (prediluted to a concentration of 2000 μg ml⁻¹ total protein) in PBS-T containing 1% SureBlock™. Plates were washed 5 times with PBS-T and incubated for 1 h at 25°C with 20 μl of biotinylated POM19 (used at 1:10,000 dilution in 1% SureBlock™ PBS-T). After washing the plates again with PBS-T, they were probed with horseradish peroxidase-Streptavidin (BD Biosciences; used at 1:1000 dilution in 1% SureBlock™, PBS-T). Following the final washing step, plates were incubated for 10 min with TMB stabilizing chromogen (Invitrogen) and developed using 0.5 M sulphuric acid. The optical density was measured at 450 nm using an EnVision Platereader. Using the rmPrP standard curve, we interpolated the values of the brain homogenates to calculate PrP concentration per sample. Following these steps, the PrP concentrations obtained for each sample were normalized to the respective concentrations of the tissue homogenates of Bl6 (positive control) and ZH3 (negative control) mice in order to counterbalance potential assay-to-assay heterogeneity. We thus show PrP levels as percentages relative to Bl6 PrP expression.

To analyse lysate under deglycosylation conditions, homogenates were incubated with PNGaseF (NewEngland Biolabs) following the manufacturer's instructions. For Western blotting, equal amounts (25 μg protein) of cell or COCS homogenate with or without PNGaseF digestion were mixed with loading dye (ThermoScientific) and loaded on a 4%–12% precast NuPage gel (Invitrogen). Transfer to a PVDF membrane (Invitrogen) was performed using a iBlot™ Cel Transfer Device. PrP^C was detected by Western blot using the monoclonal antibody POM19 at 0.1 μg ml⁻¹. NeuN was detected by using anti-NeuN (D3S3I) antibodies. Loading control was performed with anti-α-GAPDH (Sigma-Aldrich, 1:15,000). Horseradish peroxidase (HRP) goat anti-rabbit or mouse IgG1 (1:10,000, Zymed) was used as secondary antibody. Membranes were illuminated using a Stella Imaging System.

4.12 | Immunostaining of COCS

COCS grown on PTFE were washed twice in PBS and fixed in 4% paraformaldehyde for at least 2 days at 4°C and were washed again twice in PBS prior to blocking of unspecific binding by incubation in blocking buffer (0.05% Triton X-100 vol/vol, 0.3% goat serum vol/vol in PBS) for 1 h at room temperature. The primary antibody was dissolved in blocking buffer and incubated for 3 days at 4°C. After three washes with PBS for 30 min, COCS were incubated for 3 days at 4°C with fluochrome conjugated secondary antibodies at a dilution of 1:1000 in blocking buffer. Slices were then washed with PBS for 15 min and incubated in DAPI (1 μg ml⁻¹) in PBS at room temperature for 30 min to visualize cell nuclei. Two subsequent washes in PBS were performed and COCS were mounted with fluorescence mounting medium (DAKO) on glass slides. Pearson's correlation coefficient was calculated using the macro JACoP [60] after background subtraction in Fiji.

4.13 | Propidium iodide (PI) staining of COCS

For propidium iodide (PI, Sigma) staining of COCS cultured on cover slips, PI was diluted in slice culture media at a final concentration of 10 μM. The media in roller tubes were replaced by media containing 10 μM of PI solution and slices were incubated for 30 min. After incubation, the media were replaced with fresh media and returned to the incubator for 10 min prior to imaging with Olympus FLUOVIEW as described above.

For COCS cultured on PTFE membranes 1 ml of media containing PI solution (10 μM). PTFE membranes with COCS were placed into the solution and incubated at room temperature for 30 min, covered with aluminium. Subsequently, petri dishes containing stained COCS on membrane were imaged with Olympus Fluoview (excitation maximum: 534 nm; emission maximum: 617).

4.14 | Simulation details

All molecular dynamics simulations were performed using the GROMACS simulation package [61] and the CHARMM36 force field [62] with the TIP3P water model. Most simulations were carried out with the 3-octapeptide repeat (residues 60–83) of the flexible tail (FT) of PrP^C except for a run with residues 23–90. The DPPC (dipalmitoylphosphatidylcholine) bilayer was prepared using the GROMACS simulation package [61]. Equilibration consisted of 10 ns. During both the equilibration and production runs, van der Waals interactions were switched off at a distance of 1.0 nm and electrostatic short-range interactions were cut-off beyond a distance of 1.2 nm. The long-range electrostatic interactions were

treated with Particle Mesh Ewald [63]. The simulation temperature of 323 K, which is above the main phase transition of the DPPC bilayer, was kept constant using the v-rescale algorithm [63]. The Berendsen pressure coupling algorithm [30] was employed for constant pressure simulation at 1 atm. Periodic boundary conditions were applied. All simulations started with the peptide at a distance of at least 1.5 nm from the bilayer surface. Four independent simulations with different initial velocities were carried out for the wt and three simulations for the triple-point mutant. The length of each run was between 170 and 410 ns (see Figure S7) and snapshots were saved every 50 ps. A time step of 2 fs was employed for all runs.

4.15 | Statistical analysis

The two-way ANOVA Sidak post hoc test for multicolour comparisons or the Dunnett's post-hoc test for comparisons of all columns to a control column were used for statistical analysis of experiments involving the comparison of three or more samples. A paired Student's *t*-test was used for comparing two samples. Results are displayed as the average of replicates \pm SD. Significance is defined as a *p* value below 0.05.

AUTHOR CONTRIBUTIONS

Regina R. Reimann designed, supervised and coordinated the research and developed the assay, performed validation experiments of the assay with the assistance of Martina Puzio and Antonella Rosati, cloned the polyprotein vector and the vectors for expression of mutant PrP^C (70%) with Antonella Rosati (30%), determined the functional AAV titre after production (60%) with Antonella Rosati (40%), checked expression of mutated prion protein in cells (30%) together with Antonella Rosati (70%), modified a previously established ELISA protocol for determining protein expression level together with Marc Emmenegger, performed anti-prion antibody treatment and imaging of COCS cultured on cover-slips (50%) with Antonella Rosati (30%) and Martina Puzio (20%), analysed data and wrote the manuscript with Adriano Aguzzi. Martina Puzio performed validation experiments of the assay, performed anti-prion antibody treatment and imaging of COCS (20%) and analysed data. Antonella Rosati performed validation experiments of the assay, helped with the cloning of the vectors for expression of mutant PrP^C (30%), determined the functional AAV titre (40%), determined protein expression level by ELISA, produced and transduced COCS, performed anti-prion antibody treatment and imaging of COCS cultured on cover-slips (30%). Marc Emmenegger modified a previously established ELISA for determining protein expression level and edited the manuscript. Bernard L. Schneider and Pamela Valdés produced viral vectors. Danzhi Huang and Amedeo Cafilisch

performed molecular dynamic experiments and analysed data. Adriano Aguzzi conceived the primary idea of the project, advised on establishing the COCS assay, coordinated the research tasks, appropriated the funding, offered feedback and mentoring, and wrote and edited the paper.

ACKNOWLEDGMENTS

We thank Livia Takács, Ahmet Varol and Linda Irpino for technical help, Dr. Assunta Senatore for providing Fab83 and for discussions, Dr. Simone Hornemann and Prof. Ben Schuler for advice on prion protein modification, Prof. Elisabeth Rushing and Artemi Bendandi for editorial assistance, Rita Moos for production of the Fab fragments and Mirzet Delic for handling mice.

FUNDING INFORMATION

A.A. is supported by institutional core funding by the University of Zurich and the University Hospital of Zurich, the Schwyzer Winiker Stiftung, the NOMIS Foundation, and the Baugarten Stiftung (coordinated by the USZ Foundation, USZF27101), the Innovation Fund of the University Hospital Zurich (INOV00096), the Driver Grant 2017DRI17 of the Swiss Personalized Health Network (SPHN), a Distinguished Scientist Award of the NOMIS Foundation, an Advanced Grant of the European Research Council (ERC Prion2020 No. 670958) and grants from the GELU Foundation, the Swiss National Science Foundation (SNSF grant ID 179040 and grant ID 207872, Sinergia grant ID 183563), the HMZ ImmunoTarget grant, the Human Frontiers Science Program (grant ID RGP0001/2022), the Michael J. Fox Foundation (grant ID MJFF-022156), and the Innosuisse Innovation project 100.020 IP-LS. RRR was supported for this work by a Career Development Award from the Stavros Niarchos Foundation.

CONFLICT OF INTEREST

The authors declare no competing financial interests.


DATA AVAILABILITY STATEMENT

The original contribution presented in the study are included in the article/supplementary material. Any additional information/data will be made available by the corresponding author upon reasonable request.


ORCID

Regina R. Reimann  <https://orcid.org/0000-0002-6396-4195>

Martina Puzio  <https://orcid.org/0000-0002-8835-4967>

Marc Emmenegger  <https://orcid.org/0000-0002-6073-8811>

Bernard L. Schneider  <https://orcid.org/0000-0001-5485-8748>

Amedeo Cafilisch  <https://orcid.org/0000-0002-2317-6792>

Adriano Aguzzi  <https://orcid.org/0000-0002-0344-6708>

REFERENCES

- Riek R, Hornemann S, Wider G, Glockshuber R, Wuthrich K. NMR characterization of the full-length recombinant murine prion protein, mPrP(23-231). *FEBS Lett.* 1997;413(2):282–8.
- Brandner S, Isenmann S, Raeber A, Fischer M, Sailer A, Kobayashi Y, et al. Normal host prion protein necessary for scrapie-induced neurotoxicity. *Nature.* 1996;379(6563):339–43.
- Chesebro B, Trifilo M, Race R, Meade-White K, Teng C, LaCasse R, et al. Anchorless prion protein results in infectious amyloid disease without clinical scrapie. *Science.* 2005;308(5727):1435–9.
- Mallucci G, Dickinson A, Linehan J, Klohn PC, Brandner S, Collinge J. Depleting neuronal PrP in prion infection prevents disease and reverses spongiosis. *Science.* 2003;302(5646):871–4.
- Corbett GT, Wang Z, Hong W, Colom-Cadena M, Rose J, Liao M, et al. PrP is a central player in toxicity mediated by soluble aggregates of neurodegeneration-causing proteins. *Acta Neuropathol.* 2020;139(3):503–26.
- Lauren J, Gimbel DA, Nygaard HB, Gilbert JW, Strittmatter SM. Cellular prion protein mediates impairment of synaptic plasticity by amyloid-beta oligomers. *Nature.* 2009;457(7233):1128–32.
- Resenberger UK, Harmeier A, Woerner AC, Goodman JL, Muller V, Krishnan R, et al. The cellular prion protein mediates neurotoxic signalling of beta-sheet-rich conformers independent of prion replication. *EMBO J.* 2011;30(10):2057–70.
- Reimann RR, Sonati T, Hornemann S, Herrmann US, Arand M, Hawke S, et al. Differential toxicity of antibodies to the prion protein. *PLoS Pathog.* 2016;12(1):e1005401.
- Solfrosi L, Criado JR, McGavern DB, Wirz S, Sanchez-Alavez M, Sugama S, et al. Cross-linking cellular prion protein triggers neuronal apoptosis in vivo. *Science.* 2004;303(5663):1514–6.
- Sonati T, Reimann RR, Falsig J, Baral PK, O'Connor T, Hornemann S, et al. The toxicity of anti-prion antibodies is mediated by the flexible tail of the prion protein. *Nature.* 2013;501(7465):102–6.
- Wu B, McDonald AJ, Markham K, Rich CB, McHugh KP, Tatzelt J, et al. The N-terminus of the prion protein is a toxic effector regulated by the C-terminus. *Elife.* 2017;6:e23473.
- Baumann F, Tolnay M, Brabeck C, Pahnke J, Klotz U, Niemann HH, et al. Lethal recessive myelin toxicity of prion protein lacking its central domain. *EMBO J.* 2007;26(2):538–47.
- Li A, Christensen HM, Stewart LR, Roth KA, Chiesa R, Harris DA. Neonatal lethality in transgenic mice expressing prion protein with a deletion of residues 105–125. *EMBO J.* 2007;26(2):548–58.
- Shmerling D, Hegyi I, Fischer M, Blattler T, Brandner S, Gotz J, et al. Expression of amino-terminally truncated PrP in the mouse leading to ataxia and specific cerebellar lesions. *Cell.* 1998;93(2):203–14.
- Herrmann US, Sonati T, Falsig J, Reimann RR, Dametto P, O'Connor T, et al. Prion infections and anti-PrP antibodies trigger converging neurotoxic pathways. *PLoS Pathog.* 2015;11(2):e1004662.
- Karl Frontzek MB, Senatore A, Henzi A, Raimann RR, Bedir S, Marino M, et al. A conformational switch controlling the toxicity of the prion protein. *Nat Struct Mol Biol.* 2022;29(8):831–40.
- Frontzek K, Pfammatter M, Sorce S, Senatore A, Schwarz P, Moos R, et al. Neurotoxic antibodies against the prion protein do not trigger prion replication. *PLoS One.* 2016;11(9):e0163601.
- Aguzzi A, Baumann F, Bremer J. The prion's elusive reason for being. *Annu Rev Neurosci.* 2008;31:439–77.
- Jumper J, Evans R, Pritzel A, Green T, Figurnov M, Ronneberger O, et al. Highly accurate protein structure prediction with AlphaFold. *Nature.* 2021;596(7873):583–9.
- Varadi M, Anyango S, Deshpande M, Nair S, Natassia C, Yordanova G, et al. AlphaFold protein structure database: massively expanding the structural coverage of protein-sequence space with high-accuracy models. *Nucleic Acids Res.* 2022;50(D1):D439–D44.
- Kugler S, Kilic E, Bahr M. Human synapsin 1 gene promoter confers highly neuron-specific long-term transgene expression from an adenoviral vector in the adult rat brain depending on the transduced area. *Gene Ther.* 2003;10(4):337–47.
- Nuvolone M, Hermann M, Sorce S, Russo G, Tiberi C, Schwarz P, et al. Strictly co-isogenic C57BL/6J-Prnp^{0/0} mice: a rigorous resource for prion science. *J Exp Med.* 2016;213(3):313–27.
- Gahwiler BH, Thompson SM, Muller D. Preparation and maintenance of organotypic slice cultures of CNS tissue. *Curr Protoc Neurosci.* 2001;9(1):1–11. Chapter 6:Unit 6.11.
- Dametto P, Lakkaraju AK, Bridel C, Villiger L, O'Connor T, Herrmann US, et al. Neurodegeneration and unfolded-protein response in mice expressing a membrane-tethered flexible tail of PrP. *PLoS One.* 2015;10(2):e0117412.
- Shagghi N, Palombo EA, Clayton AH, Bhawe M. Archetypal tryptophan-rich antimicrobial peptides: properties and applications. *World J Microbiol Biotechnol.* 2016;32(2):31.
- Evans EG, Pushie MJ, Markham KA, Lee HW, Millhauser GL. Interaction between prion protein's copper-bound octarepeat domain and a charged C-terminal pocket suggests a mechanism for N-terminal regulation. *Structure.* 2016;24(7):1057–67.
- Schilling KM, Tao L, Wu B, Kiblen JTM, Ubilla-Rodriguez NC, Pushie MJ, et al. Both N-terminal and C-terminal histidine residues of the prion protein are essential for copper coordination and neuroprotective self-regulation. *J Mol Biol.* 2020;432(16):4408–25.
- Aronoff-Spencer E, Burns CS, Avdievich NI, Gerfen GJ, Peisach J, Antholine WE, et al. Identification of the Cu²⁺ binding sites in the N-terminal domain of the prion protein by EPR and CD spectroscopy. *Biochemistry.* 2000;39(45):13760–71.
- Bremer J, Baumann F, Tiberi C, Wessig C, Fischer H, Schwarz P, et al. Axonal prion protein is required for peripheral myelin maintenance. *Nat Neurosci.* 2010;13(3):310–8.
- Berendsen HJC, Postma JPM, von Gunsteren WF, Dinola A, Haak JR. Molecular dynamics with coupling to an external bath. *J Chem Phys.* 1984;81(8):3684.
- Senatore A, Frontzek K, Emmenegger M, Chincisan A, Losa M, Reimann R, et al. Protective anti-prion antibodies in human immunoglobulin repertoires. *EMBO Mol Med.* 2020;12(9):e12739.
- Lysek DA, Wuthrich K. Prion protein interaction with the C-terminal SH3 domain of Grb2 studied using NMR and optical spectroscopy. *Biochemistry.* 2004;43(32):10393–9.
- Balducci C, Beeg M, Stravalaci M, Bastone A, Scip A, Biasini E, et al. Synthetic amyloid-beta oligomers impair long-term memory independently of cellular prion protein. *Proc Natl Acad Sci U S A.* 2010;107(5):2295–300.
- Solomon IH, Khatri N, Biasini E, Massignan T, Huettner JE, Harris DA. An N-terminal polybasic domain and cell surface localization are required for mutant prion protein toxicity. *J Biol Chem.* 2011;286(16):14724–36.
- Westergaard L, Turnbaugh JA, Harris DA. A nine amino acid domain is essential for mutant prion protein toxicity. *J Neurosci.* 2011;31(39):14005–17.
- Vital C, Gray F, Vital A, Parchi P, Capellari S, Petersen RB, et al. Prion encephalopathy with insertion of octapeptide repeats: the number of repeats determines the type of cerebellar deposits. *Neuropathol Appl Neurobiol.* 1998;24(2):125–30.
- Chiesa R, Drisaldi B, Quaglio E, Migheli A, Piccardo P, Ghetti B, et al. Accumulation of protease-resistant prion protein (PrP) and apoptosis of cerebellar granule cells in transgenic mice expressing a PrP insertional mutation. *Proc Natl Acad Sci U S A.* 2000;97(10):5574–9.
- Chiesa R, Piccardo P, Ghetti B, Harris DA. Neurological illness in transgenic mice expressing a prion protein with an insertional mutation. *Neuron.* 1998;21(6):1339–51.

39. Flechsig E, Shmerling D, Hegyi I, Raeber AJ, Fischer M, Cozzio A, et al. Prion protein devoid of the octapeptide repeat region restores susceptibility to scrapie in PrP knockout mice. *Neuron*. 2000;27(2):399–408.
40. Marsh DR, Dekaban GA, Tan W, Strathdee CA, Weaver LC. Herpes simplex viral and amplicon vector-mediated gene transfer into glia and neurons in organotypic spinal cord and dorsal root ganglion cultures. *Mol Ther*. 2000;1(5 Pt 1):464–78.
41. Turnbaugh JA, Unterberger U, Saa P, Massignan T, Fluharty BR, Bowman FP, et al. The N-terminal, polybasic region of PrP(C) dictates the efficiency of prion propagation by binding to PrP(Sc). *J Neurosci*. 2012;32(26):8817–30.
42. Das NR, Miyata H, Hara H, Chida J, Uchiyama K, Masujin K, et al. The N-terminal polybasic region of prion protein is crucial in prion pathogenesis independently of the octapeptide repeat region. *Mol Neurobiol*. 2020;57(2):1203–16.
43. Khalife M, Reine F, Paquet-Fifield S, Castille J, Herzog L, Vilotte M, et al. Mutated but not deleted ovine PrP(C) N-terminal polybasic region strongly interferes with prion propagation in transgenic mice. *J Virol*. 2016;90(3):1638–46.
44. Kuffer A, Lakkaraju AK, Mogha A, Petersen SC, Airich K, Doucerain C, et al. The prion protein is an agonistic ligand of the G protein-coupled receptor Adgrg6. *Nature*. 2016;536(7617):464–8.
45. Goniotaki D, Lakkaraju AKK, Shrivastava AN, Bakirci P, Sorce S, Senatore A, et al. Inhibition of group-I metabotropic glutamate receptors protects against prion toxicity. *PLoS Pathog*. 2017;13(11):e1006733.
46. Kim Y, Lee J, Lee C. In silico comparative analysis of DNA and amino acid sequences for prion protein gene. *Transbound Emerg Dis*. 2008;55(2):105–14.
47. Linsenmeier L, Mohammadi B, Shafiq M, Frontzek K, Bar J, Shrivastava AN, et al. Ligands binding to the prion protein induce its proteolytic release with therapeutic potential in neurodegenerative proteinopathies. *Sci Adv*. 2021;7(48):eabj1826.
48. Linsenmeier L, Altmeyen HC, Wetzel S, Mohammadi B, Saftig P, Glatzel M. Diverse functions of the prion protein – does proteolytic processing hold the key? *Biochim Biophys Acta Mol Cell Res*. 2017;1864(11 Pt B):2128–37.
49. Zhang H, Yang B, Mu X, Ahmed SS, Su Q, He R, et al. Several rAAV vectors efficiently cross the blood-brain barrier and transduce neurons and astrocytes in the neonatal mouse central nervous system. *Mol Ther*. 2011;19(8):1440–8.
50. Fischer M, Rulicke T, Raeber A, Sailer A, Moser M, Oesch B, et al. Prion protein (PrP) with amino-proximal deletions restoring susceptibility of PrP knockout mice to scrapie. *EMBO J*. 1996;15(6):1255–64.
51. Mahal SP, Baker CA, Demczyk CA, Smith EW, Julius C, Weissmann C. Prion strain discrimination in cell culture: the cell panel assay. *Proc Natl Acad Sci U S A*. 2007;104(52):20908–13.
52. Bardelli M, Frontzek K, Simonelli L, Hornemann S, Pedotti M, Mazzola F, et al. A bispecific immunotweezer prevents soluble PrP oligomers and abolishes prion toxicity. *PLoS Pathog*. 2018;14(10):e1007335.
53. Engler C, Kandzia R, Marillonnet S. A one pot, one step, precision cloning method with high throughput capability. *PLoS One*. 2008;3(11):e3647.
54. Rohr UP, Heyd F, Neukirchen J, Wulf MA, Queitsch I, Kroener-Lux G, et al. Quantitative real-time PCR for titration of infectious recombinant AAV-2 particles. *J Virol Methods*. 2005;127(1):40–5.
55. Polymenidou M, Moos R, Scott M, Sigurdson C, Shi YZ, Yajima B, et al. The POM monoclonals: a comprehensive set of antibodies to non-overlapping prion protein epitopes. *PLoS One*. 2008;3(12):e3872.
56. Williamson RA, Peretz D, Pinilla C, Ball H, Bastidas RB, Rozenshteyn R, et al. Mapping the prion protein using recombinant antibodies. *J Virol*. 1998;72(11):9413–8.
57. Hornemann S, von Schroetter C, Damberger FF, Wuthrich K. Prion protein-detergent micelle interactions studied by NMR in solution. *J Biol Chem*. 2009;284(34):22713–21.
58. Falsig J, Julius C, Margalith I, Schwarz P, Heppner FL, Aguzzi A. A versatile prion replication assay in organotypic brain slices. *Nat Neurosci*. 2008;11(1):109–17.
59. Emmenegger M, De Cecco E, Hruska-Plochan M, Eninger T, Schneider MM, Barth M, et al. LAG3 is not expressed in human and murine neurons and does not modulate alpha-synucleinopathies. *EMBO Mol Med*. 2021;13(9):e14745.
60. Bolte S, Cordelieres FP. A guided tour into subcellular colocalization analysis in light microscopy. *J Microsc-Oxford*. 2006;224:213–32.
61. Van Der Spoel D, Lindahl E, Hess B, Groenhof G, Mark AE, Berendsen HJ. GROMACS: fast, flexible, and free. *J Comput Chem*. 2005;26(16):1701–18.
62. Huang J, Rauscher S, Nawrocki G, Ran T, Feig M, de Groot BL, et al. CHARMM36m: an improved force field for folded and intrinsically disordered proteins. *Nat Methods*. 2017;14(1):71–3.
63. Darden T, York D, Pedersen L. Particle mesh Ewald: an N-log(N) method for Ewald sums in large systems. *J Chem Phys*. 1993;98(12):10089–92.

SUPPORTING INFORMATION

Additional supporting information can be found online in the Supporting Information section at the end of this article.

How to cite this article: Reimann RR, Puzio M, Rosati A, Emmenegger M, Schneider BL, Valdés P, et al. Rapid ex vivo reverse genetics identifies the essential determinants of prion protein toxicity. *Brain Pathology*. 2022. e13130. <https://doi.org/10.1111/bpa.13130>